Engineering Structures 280 (2023) 115715

Contents lists available at ScienceDirect

Engineering Structures

journal homepage: www.elsevier.com/locate/engstruct

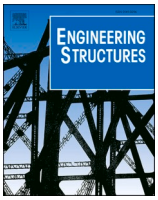

Wave characteristics of reconfigurable elastic metamaterials based on a multi-stable structure

Meng Chen [a,b], Boya Xiao [a,b], Yafei Feng [c], Tao Yang [a,b], Han Zhang [d], Yu Liu [a,b], Wenshuai Xu [a,b], Heng Jiang [a,b,*], Yuren Wang [a,b]

[a] Key Laboratory of Microgravity, Institute of Mechanics, Chinese Academy of Sciences, Beijing 100190, China
[b] University of Chinese Academy of Sciences, Beijing 100049, China
[c] Units 92228 of Chinese People's Liberation Army, Beijing 100072, China
[d] Noise and Vibration Laboratory, Institute of Acoustics, Chinese Academy of Sciences, 100190 Beijing, China

ARTICLE INFO

Keywords:
Reconfigurable elastic metamaterials
Multi-stable structure
Bandgap
Local resonance
Waveguide

ABSTRACT

Elastic metamaterials have been considered as important tools for vibration and noise reduction because of their subwavelength bandgaps. However, acritical problem hindering their practical application is the difficulty of constructing an adjustable unit cell that facilitates bandgap tuning. In this study, reconfigurable two-dimensional metamaterials based on four curved beams are developed such that they could sustain multi-stable configurations. Our calculations and experiments reveal that the developed unit cell can exhibit bidirectional phase transformations to three stable configurations. The three stable configurations have different wave characteristics, allowing for elastic wave propagation to be tuned at the subwavelength scale. Based on this tuneability, a waveguide can be designed and the wave direction of travel can be controlled. This study provides a novel approach for designing reconfigurable elastic wave materials, elastic wave logic circuits, and waveguides.

1. Introduction

In recent years, elastic metamaterials have generated considerable interest as artificial period materials owing to their supernormal physical properties [1–5] and strong designability [6,7]. One of their most useful properties is their bandgap [8–23], a frequency range in which the propagation of elastic waves is prevented. This ability to arrest wave propagation leads to potential applications in waveguides or vibration and noise reduction [6,7,24,25]. Most studies on elastic metamaterials were focused on microstructural cell designs [10–18], bandgap formation mechanisms [19–23], and property-influencing factors [8,9]. However, the working frequencies of these materials are usually fixed after unit cell design, considerably restricting the use of such materials in intelligent applications [26–28]. Thus, the construction of a tunable unit cell that allows for the active regulation of various frequency ranges has become a primary goal in metamaterial research.

The working frequency of elastic metamaterials depends on both the mechanical properties and geometric structures of the component materials [19–23,29–32]. Tuning strategies can be classified into two major categories. The first involves the incorporation of active materials, such as magnetorheological/electrorheological [33,34], piezoelectric [34–37], electromagnetic [38,39], and nonlinear materials [40–42], which are sensitive to external stimuli and enable the dynamic control of stiffness or resonator mass. The second approach involves the use of external stimuli to reconfigure a material's geometric structure, for example by changing its lattice constant [43,44], resonator shape, or spatial arrangement [45–47]. In contrast to active material addition, geometric reconfiguration under an external force is straightforward, but both categories of adjustment require continuous external excitation. In other words, maintaining tuned metamaterials in a stable state requires a sustained external stimulus that induces changes in the material's parameters or configuration [48]. Therefore, designing metamaterials that have reversible and stable configurations is crucial.

Multi-stable mechanical metamaterials are artificial structures with two or more interchangeable stable configurations [49–55]. These stable configurations correspond to energetic minima in a system, indicating that diverse stable configurations can be maintained even after the external load or other stimuli are removed [54,55]. Several recent studies suggest that the use of multi-stable mechanical metamaterials represent a new approach for achieving tunable elastic metamaterials

* Corresponding author.
E-mail address: hengjiang@imech.ac.cn (H. Jiang).

https://doi.org/10.1016/j.engstruct.2023.115715

Available online 6 February 2023

[48,56–66]. For instance, Meaudet al. designed reconfigurable materials based on a one-dimensional (1D) chain of bistable unit cells and analyzed the propagation of elastic waves as acoustic switches [56]. Valencia et al. analyzed planar wave propagation in a 1D periodic multi-stable cellular material, showing that it exhibits highly anisotropic wave propagation behavior [59]. In other studies, tunable elastic meta-materials with multi-stable structures, based on shape memory poly-mers, were prepared by applying four-dimensional (4D) printing, and their bandgaps were adjusted by changing external forces and temper-atures [48,61]. Although multi-stable two-dimensional (2D) meta-materials employing a mass-spring model [62–64] or modular multi-stable metamaterials [65,66] have been proposed, investigations in to tunable 2Dmetamaterials with multi-stable configurations are lacking. In addition, a local resonance mechanism is required to improve the controllability of low-frequency waves at the subwavelength scale.

Compared with the geometrical frustration, snap-through, and structured mechanisms, developing a unit cell of multi-stable meta-materials composed of curved beams represents a simpler approach [49]. In this study, reconfigurable 2Dmetamaterials were developed by using four curved beams such that they could sustain multi-stable con-figurations. To introduce the local resonance mechanism, a large mass block was placed in the middle of the four symmetrical curved beams. The calculations and experiments performed revealed that the unit cell designed in this study can undergo bidirectional phase transformations to three stable configurations. All three configurations were verified to have different wave characteristics, allowing for the tuning of elastic wave propagation. The propagation characteristics of the elastic waves in the different stable states of reconfigurable elastic metamaterials (REMs) indicate that elastic wave behavior can be modulated by switching different states under a force at the subwavelength scale. Compared with previous approaches, the use of REMs offers greater design versatility, allowing for finer tuning of elastic wave propagation. This tuneability can facilitate the design of a waveguide that can control to the travel of waves in a particular direction.

2. Geometric configuration and numerical calculation method

2.1. Design of the bistable curved beam

Fig. 1 shows a diagram of a bistable curved beam, indicating how it may be used to achieve multistable configurations. Here, the curved beam is fixed at both ends and can be switched between two stable positions, Stages I and II, by applying an external force to its middle. Equation (1) describes the initial shape of a curved sinusoidal beam [66,67]:

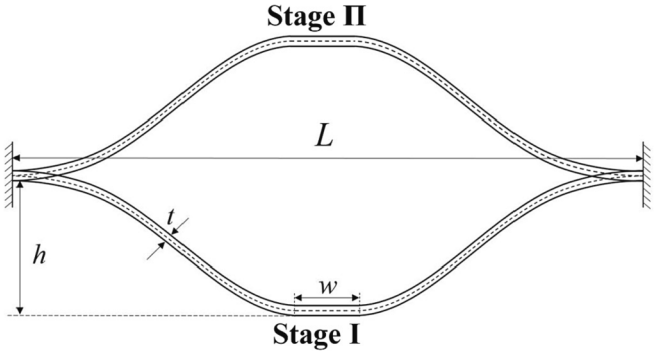

Fig. 1. Schematic Diagram of Bistable Curved Beam.

$$h(x)=\begin{cases}\dfrac{h}{2}\times\left[1+\cos\left(\dfrac{2\pi x}{L-W}\right)\right], x\in\left[0,\dfrac{L-W}{2}\right]\\ 0, x\in\left[\dfrac{L-W}{2},\dfrac{L+W}{2}\right]\\ \dfrac{h}{2}\times\left[1-\cos\left(\dfrac{2\pi(x-\frac{L+W}{2})}{L-W}\right)\right], x\in\left[\dfrac{L+W}{2},L\right]\end{cases} \tag{1}$$

According to the literature, the relationship between the external force and the displacement of this curved beam can be expressed by Equations (2)–(4) [67,68]:

$$F=\frac{3\pi^4Q^2}{2}\left(\Delta-\frac{3}{2}+\sqrt{\frac{1}{4}-\frac{4}{3Q^2}}\right)\left(\Delta-\frac{3}{2}-\sqrt{\frac{1}{4}-\frac{4}{3Q^2}}\right) \tag{2}$$

$$F=\frac{f(L-W)^3}{EIh} \tag{3}$$

$$\Delta=\frac{d}{h} \tag{4}$$

where f is the external force, d is the deflection at the center of the beam, F is the dimensionless force (f), Δ is the dimensionless displace-ment (d), h is the initial apex height of the beam, E is the Young's modulus of the raw material, and L is the span of the curved beam. Q is a geometric constant defined as the ratio of the beam height to thickness ($Q = h / t$), which is critical for bistable behavior [68]. When Q is suf-ficiently large, the curved beam exhibits multiple stable states. When Q is small, however, the force is always positive and only the initial shape is stable. Based on the results obtained in previous works, $Q = 5$ ($h = 2.5$ mm, $t = 0.5$ mm) was selected when designing the multi-stable structure described in this study.

2.2. Design of subwavelength REMs

The unit cell of the REMs can be designed by symmetrically distributing curved beams in the x- and y-directions, as illustrated in Fig. 2(a). The material has a simple square lattice structure with a square unit cell composed of four curved beams joined by four rectangles of equal length, l, and thickness, W, as shown in Fig. 2(b). The middle is a square mass block and the lattice constant is a. The entire structure has multistable states under axial force in the x- and y-directions owing to the bistable curved beam. Based on their dynamic behaviors and low stiffness, curved beams can also act as springs. Thus, the entire structure described earlier is a typical local resonance system that can control elastic waves at a subwavelength scale [10]. Compared with previously reported 1D structures, the unit cell described here can be reconfigured in two directions and allows for finer elastic wave propagation tuning [48,56–68].

The structural parameter settings used in the current design are as follows: span of the curved beam is $L = 52.0$ mm, initial apex height of the beam is $h = 2.5$ mm, thickness is $t = 0.5$ mm, thickness of rectangle is $W = 16.0$ mm, length of rectangle is $l = 24.0$ mm, and lattice constant is $a = 107.0$ mm. Note that traditional multi-stable metamaterials are usually polymeric. However, to improve mechanical performance, the entire structure used in this study was made of a NiTi alloy with a density of $\rho = 6.395$ g/cm^3 and a Young's modulus of $E = 63.28$ GPa.

2.3. Numerical calculation method

The multi-stable performances, bandgaps, vibration modes, and transmission losses of the REMs were evaluated by using finite element methods (FEMs) in the COMSOL Multiphysics software package [69]. When the multi-stable performance was investigated, the lower boundary was a fixed boundary condition, the left and right boundaries

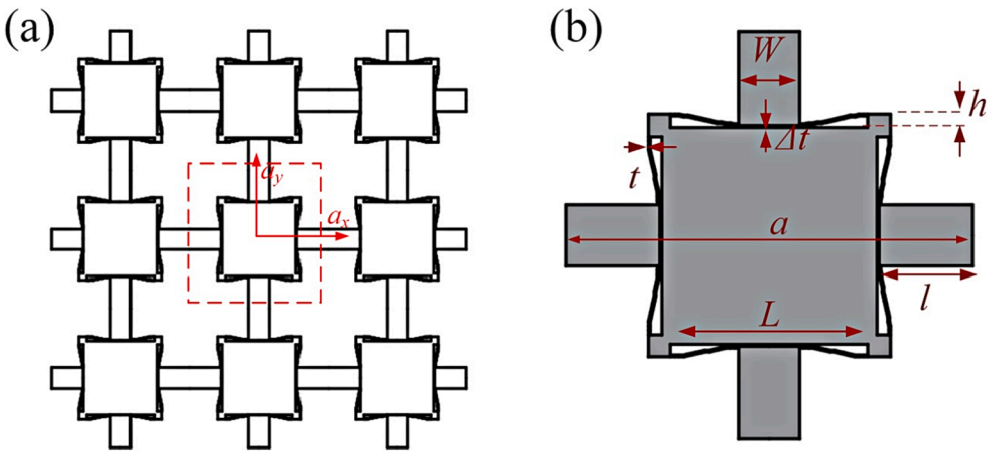

Fig. 2. (a) Structural Layout and (b) Unit Cell of REMs.

were roller supports, and upward tension was applied to the upper boundary. Each stable state was determined by extracting the force–displacement curve during tensile testing. When the dispersion relations of the REMs were determined, only fluctuations in the *x*-*y* plane were considered. Based on Bloch's theorem, periodic boundary conditions were imposed on the opposing boundaries of the unit cell [70] as follows:

$$\begin{aligned} u(x+a,y) &= u(x,y)e^{i(k_x\cdot a)},\\ v(x+a,y) &= v(x,y)e^{i(k_x\cdot a)}.\\ u(x,y+a) &= u(x,y)e^{i(k_y\cdot a)},\\ v(x,y+a) &= v(x,y)e^{i(k_y\cdot a)}. \end{aligned} \tag{5}$$

The entire band structure was obtained by sweeping the wave vector along the edges of the irreducible Brillouin zone. The effective parameter values of the medium were calculated by determining the displacement, strain, stress, and force on the boundaries, using calculation methods taken from the literature [71]. The effective mass density of the unit cell was determined from the average reaction force at the four boundaries by applying the following equation:

$$\rho_{eff} = \frac{1}{s}\frac{F_i}{\ddot{U}_i}, (i,j=1,2), \tag{6}$$

where F_i is the resultant force on the boundaries, $\ddot{U}_i$ is the average acceleration, and S is the area of the unit cell. The effective moduli were investigated under the following global hydrostatic deformation conditions:

$$E_b = \varepsilon^0\begin{bmatrix}1 & 0\\ 0 & 1\end{bmatrix}, \tag{7}$$

where E_b is the strain field at the boundary node of the unit cell. The global stress components, $\sum_{ij}$ and E_{ij}, were averaged over the external boundary by using the expression:

$$\sum_{ij} = \frac{1}{S}\int_{\partial S}\sigma_{im}x_j n_m dl, Eij = \frac{1}{2s}\int_{\partial S}(u_i n_j + u_j n_i)dl \tag{8}$$

where σ_{ij} is denotes the stress, x_j is denotes the position vector, and n_i is denotes the normal boundary unit cell.

Finally, the effective bulk moduli were obtained as

$$K_{eff} = \frac{1}{2}(\sum_{11} + \sum_{22})/(E_{11}+E_{12}). \tag{9}$$

When the transmission loss was calculated, finite elements were considered in one direction, and an infinite array of units was considered by using periodic boundary conditions in the other. Based on the assumption that the incident plane wave was applied vertically on the boundary, the transmission loss of the REMs structure can be determined by using the frequency response function (FRF). To ensure accuracy, the maximum element size of the triangular mesh was considerably less than 1/5th of the shortest wavelength in the calculated range of frequencies, and mesh refinement was performed for the curved beams. Note that the geometric parameters varied for different steady states and residual stress was not considered.

3. Results and discussion

3.1. Multi-stable performance of REMs

To verify the reconfigurability of the structure, experiments and calculations were performed to investigate the structures multi-stable characteristics. As a result of their symmetry, all four beams had the same force–displacement curve. During the test, the middle position of the cell was fixed and tension was applied to one of the four curved beams. Fig. 3 displays the obtained force–displacement curves, which show that as pull-up displacement increases, the force value first increases during the positive stiffness stage. The load then increases with displacement, and a snap-through occurs. Subsequently, the force values start to decrease with increasing displacement, and the overall stiffness of the structure becomes negative as it enters its negative-stiffness stage. The complete stretching process can, therefore, be divided into two

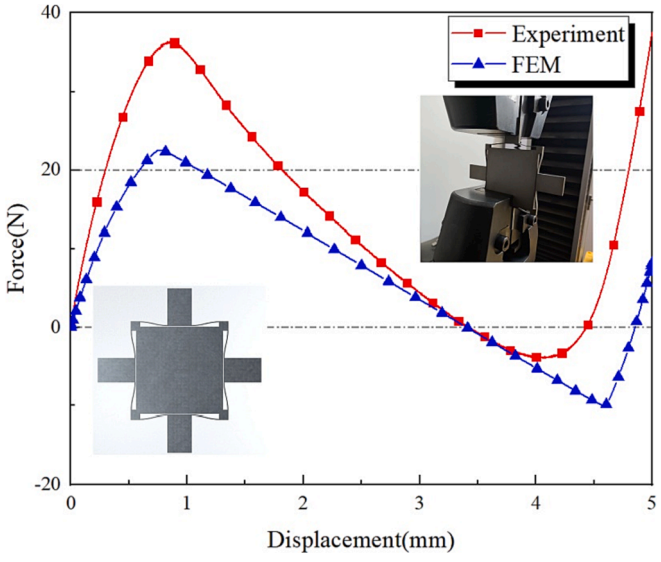

Fig. 3. Force-Displacement Curves in Experiments versus Calculations.

stages. If the force value continues to decrease until it becomes negative, a bistable phenomenon occurs [66,67]. In the study of REMs, both calculation sand experiments show that peak stress is negative, which reveals the bistable characteristics of the structure [67]. Thus, when stress is negative, the structure enters a stable locking state, and even when the external force is removed, the structure cannot revert to its original shape. According to symmetry considerations, the REM has three stable states: four bending beams in compression (state 00), four bending beams in tension (state 11), and two beams under tension in one direction and two beams under compression in the other (state 01). Switching back and forth between these states is possible by applying an external force, allowing for reconfigurable adjustments to be made. However, a noticeable difference exists between the experimental and calculated results, which might be caused by a small deviation in structure during the manufacturing process.

3.2. Band structure and vibration modes of REMs

FEMs were applied to analyze the bandgaps and vibration modes of the REMs in three stable states. The results of this analysis are shown in Figs. 4 and 5. As shown in Fig. 4, the dispersion curves of the three states are different. Fig. 4(a) shows that for state 00, three complete bandgaps are present with frequency ranges of 295.29–572.25 Hz, 706.23–3722.5 Hz, and 4015.9–4781.5 Hz. The first bandgap lies between the third and fourth dispersion curves. The second bandgap lies between the fifth and sixth dispersion curves. The third bandgap lies between the seventh and eighth dispersion curves. Fig. 4(b) shows that for state 11, two bandgaps exist at the calculated frequency ranges of 324.26–632.6 Hz and 774.18–4156.6 Hz. As in state 00, the first bandgap here also lies between the third and fourth dispersion curves, and the second bandgap lies between the fifth and sixth dispersion curves. Compared with state 00, the first and second bandgaps of state 11 are shifted toward higher frequencies, and the second bandgap is wider. Fig. 4(c) shows that for state 01, the dispersion curves can be considered as a hybrid state composed of states 00 and 11, with three bandgaps located at 326.46–596.28 Hz, 745.64–3757.2 Hz, and 3861.6–4285.2 Hz. In addition, residual stress often exists in the REMs when different states are switched. The band structures under different internal stresses are calculated, as shown in Supplementary Material. The results show that the internal stress has no effect on the bandgap for REMs with linear materials.

These calculations confirmed that all three states can achieve effective isolation of elastic waves over a wide frequency range. In the frequency range of 0–5000 Hz, the bandgap of state 00 accounts for 81 %, that of state 01accounts for 74 %, and that of state 11 accounts for 73 %, which shows the good vibration isolation property of REMs. When compared with traditional lattice structures or three-component metamaterials, the materials described in this study exhibit broad-band properties. In addition, the wavelengths of the longitudinal wave corresponding to the center frequencies of the three bandgaps for state 00 are 7.250 m, 1.400 m, and 0.710 m for 295.29–572.25 Hz, 706.23–3722.5 Hz, and 4015.9–4781.5 Hz, respectively, and the lattice size for state 00 is 0.107 m. This comparison indicates that REMs form bandgaps at subwavelength scales and that these bandgaps may form as a result of local resonance mechanisms.

To further verify the bandgap formation mechanism of the REMs and analyze the physical implications of the differences between the bandgaps of states 00 and 11, the vibration modes at the cutoff frequency were investigated. In Fig. 5, the vibration modes at points A, B, C, and D in Fig. 4(a) and E, F, G, and H in Fig. 4(b) are shown. For the vibration mode at the lower cutoff frequency of the first bandgap, only the internal mass block vibrates while the four supporting rectangles remain stationary, meaning the bending beam can be thought of as a spring. This vibration mode is the same as the vibrational form of a three-component acoustic metamaterial [72], which is a typical dipole. As for the vibration mode at the upper cutoff frequency of the first bandgap, the internal central mass block remains stationary while the four support beams vibrate relatively, meaning this mode can be thought of as a typical quadrupole. The negative effective mass density formed by the dipole prevents elastic waves in the frequency range from propagating through the structure, thereby giving rise to a bandgap. The vibration modes at the cutoff frequencies of the second and third bandgaps were observed to no longer be dominated by translation. In these modes, the central mass block remained stationary while the four supporting beams rotated around the center. This bandgap formation mechanism here is similar to that of the second bandgap in star-shaped metamaterials, in which the bandgap forms due to a negative effective bulk modulus induced by rotational deformation. By comparison, the vibration modes of states 00 and 11 at the first and second bandgaps were observed to be identical. The first bandgap was caused by *translation-induced* local resonance, where as the second bandgap was caused by *rotation-induced* local resonance. As the bending beam in the tensile and compressive states contributes to different stiffnesses, the cutoff frequency of the bandgap is also distinct, and, hence, the bandgap frequency shifts to a higher range in the 11 tensile state. In addition, the vibration modes at point M on the seventh-branch dispersion curve for states 00 and 11 exemplify the distinctive differences between the two and confirm the reason for the disappearance of the third bandgap in state 11.

Fig. 6 presents the effective mass density and effective bulk modulus obtained by FEMs at state 00 and 11. When the frequency corresponds with the band gap in the × direction, a negative mass density exists for state 00. Meanwhile, a negative mass density exists for state 11 when the frequency corresponds with its bandgap. The effective bulk moduli of states 00 and 11 are found to be negative in the frequency range of 3600–4600 Hz, as shown in Fig. 6(b). The results of the effective medium parameter calculations are consistent with calculations of the bandgap and vibration modes. This further confirms that the first bandgap is caused by translation-induced local resonance, whereas the second bandgap is caused by rotation-induced local resonance, as previously suggested. These local resonance modes are more conducive to the generation of a low-frequency bandgap, thus allowing elastic waves

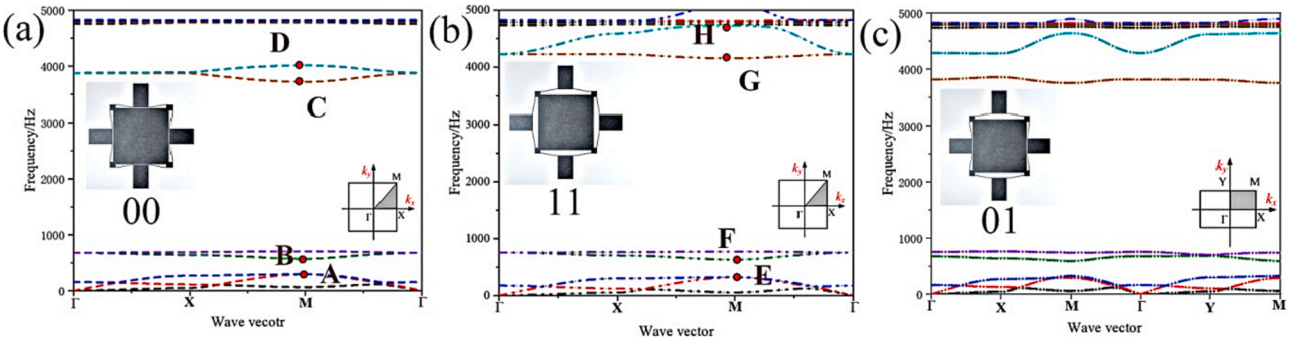

Fig. 4. Band Structure at (a) State 00, (b) State 11, and (c) State 01.

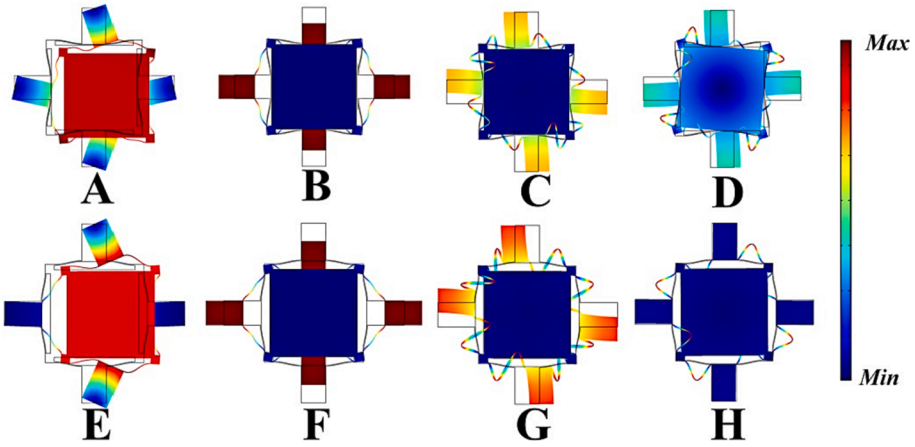

Fig. 5. Vibration Modes Corresponding to the Eigenstate Marked "A, B, C, D" at State 00and "E, F, G, H" at State 11.

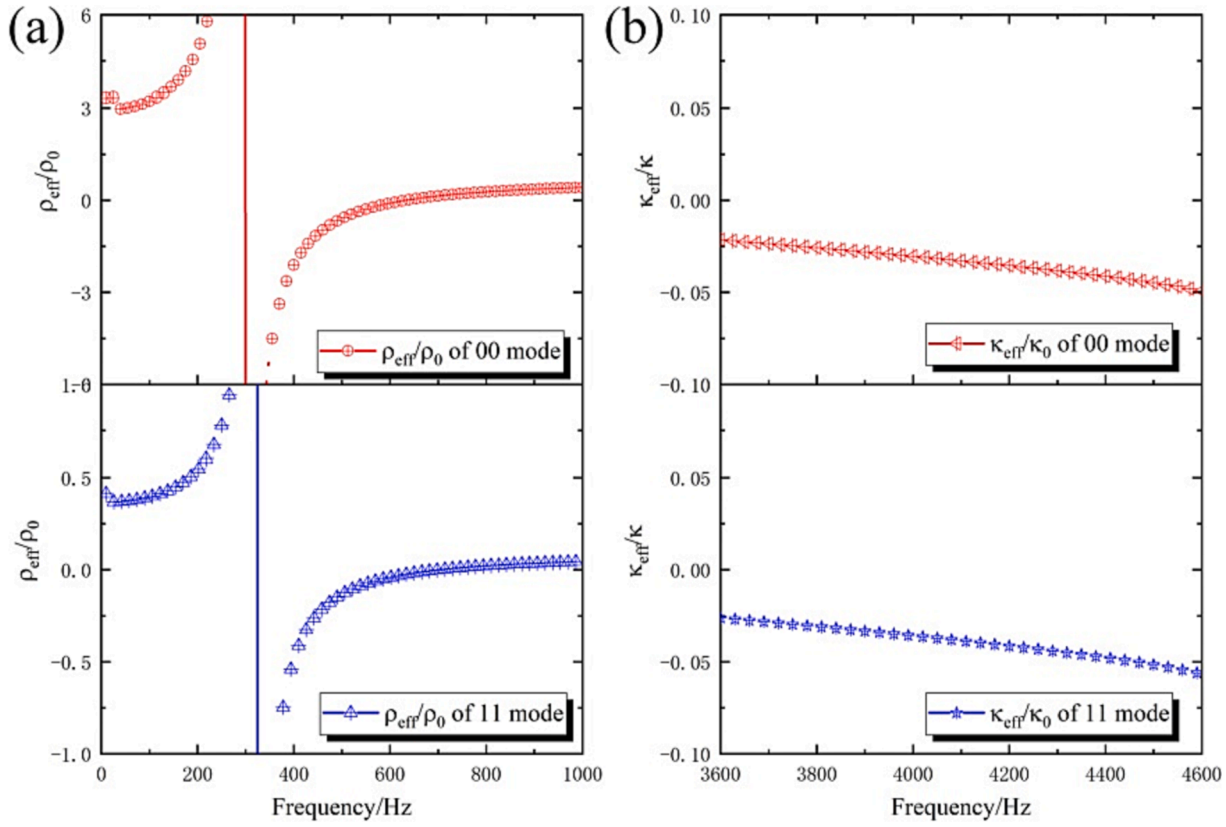

Fig. 6. (a) Effective Mass Density and (b) Effective Bulk Modulus at States 00 and 11.

at the sub-wavelength scale to be controlled.

3.3. Transmission characteristics of REMs

Next, to validate the bandgap and modal calculations, the FRF was employed by using a model composed of 3 × 5 cells, as shown in Fig. 7. The number of unit changes did not have a significant effect on transmission. In the calculation, periodic boundary conditions were applied to the upper and lower boundaries to indicate infinity in one direction, and a normal acceleration was applied to the left boundary. The transmission loss was obtained by collecting the acceleration at the right boundary. During the calculation, a perfect boundary layer was also exerted on the right side to prevent reflections caused by the interface. The calculation results show that the bandgap frequency range of the transmission loss matches that of the band structure. States 00 and 01 displayed three bandgaps, where as state 11 displayed only two. When compared with state 00, the bandgap frequency of state 11was shifted to a higher range. This reveals that REMs exhibit different transmission losses when in different stable states, allowing them to be used for force-tunable elastic waveguide switches. For example, elastic waves at a frequency of 600 Hz lie in the bandgap frequency range of state 00 and in the passband frequency range ofstates01 and 11. When the REMs in state 00 are stretched to state 01 or state 11, previously blocked elastic waves will be allowed to propagate through the structure. These two states can be switched back and forth.

To verify the tenability of the REMs for elastic wave propagation, elastic wave transmission loss was studied in different stable states. As shown in Fig. 8(a), a vibrator (MMS-50, MeK, and YMC) is used to excite

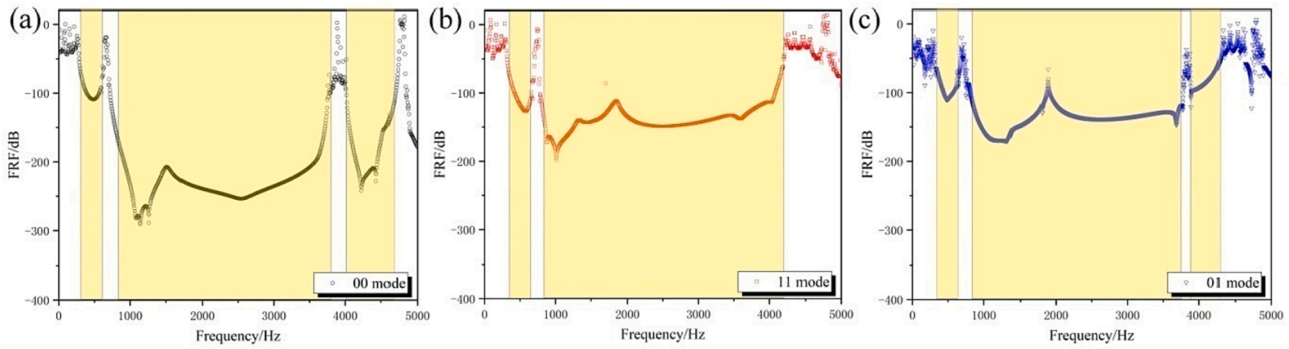

Fig. 7. FRF at (a) State 00, (b) State 11, and (c) State 01.

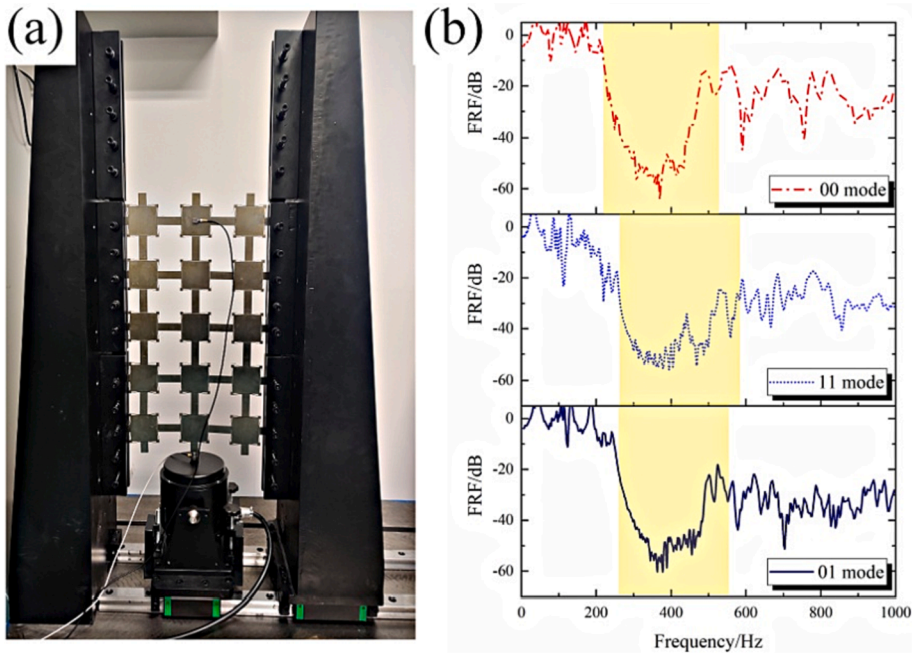

Fig. 8. (a) FRF Test Process and (b) Experimental Results.

REMs composed of 3 × 5 units in the frequency range of 10–1000 Hz, with the acceleration signal being collected at the top end using an accelerometer (B&K32602). Initially, the 3 × 5 units were all in state 00. Once the test of state 00 was completed, tension was applied to the units such that the state switched to 01 or 11.Owing to the limitations of the used laboratory test equipment, this experiment focused on the first bandgap, and the results are shown in Fig. 8(b). The yellow area in Fig. 8 (b) indicates the first bandgap frequency range. The bandgap frequency range for state 00, state 01, and state 11 is 218.9–531.9 Hz, 259.6–555.7 Hz, and 259.2–586.5 Hz, respectively. For the three states, waves above 700 Hz also have large attenuation, which is caused by the second bandgap.

Overall, the experimental results and calculations are in good agreement. Compared with states 00 and 01, the cutoff frequency of the bandgap for state 11 is shifted to a higher range. However, the experimental results and calculations have some differences. It is difficult to guarantee the manufacturing precision of the bending beam, which is the main reason for the difference between the test and the calculation. And the material parameters may have difference between experiment and calculations. The differences in the transmission loss values in all three stable states validate the tunability of the described REM for elastic wave propagation.

3.4. Design of waveguide with REMs

Based on the demonstrable tunability of the REMs for elastic wave propagation, an elastic waveguide at a given position was designed (see Fig. 9). REMs composed of 18 × 18 units were constructed, and all of them were set to state 01 (i.e., bending beams in the *x*-direction are in compression and those in the *y*-direction in tension), as shown in Fig. 9 (a). When tensile force was applied to a given position in the *x*-direction, state 01 would transition to state 11.When pressure was applied to any position in the *y*-direction, state 01 transitioned into state 00. Therefore, state 01 of the REMs could be switched by applying different forces in different directions. Switching between states should be a column or row of units as a whole, rather than a single isolated unit, as this ensures coordination and unity of deformation. The calculations for the bandgaps revealed that elastic waves at a frequency of 590 Hz can propagate in state 00 but not in state 01. Furthermore, when a waveguide with a five-unit structure was constructed, its position could be changed by applying an external force in the *y*-direction. N represents the coordinates corresponding to the middle positions of the five units. Fig. 9(b) shows the displacement distribution for N = 10, where the elastic wave at 590 Hz can propagate only along the five units in state 00. Fig. 9(c) shows the calculation results along they-direction. The FRF curves at different positions prove that the wave at 590 Hz can

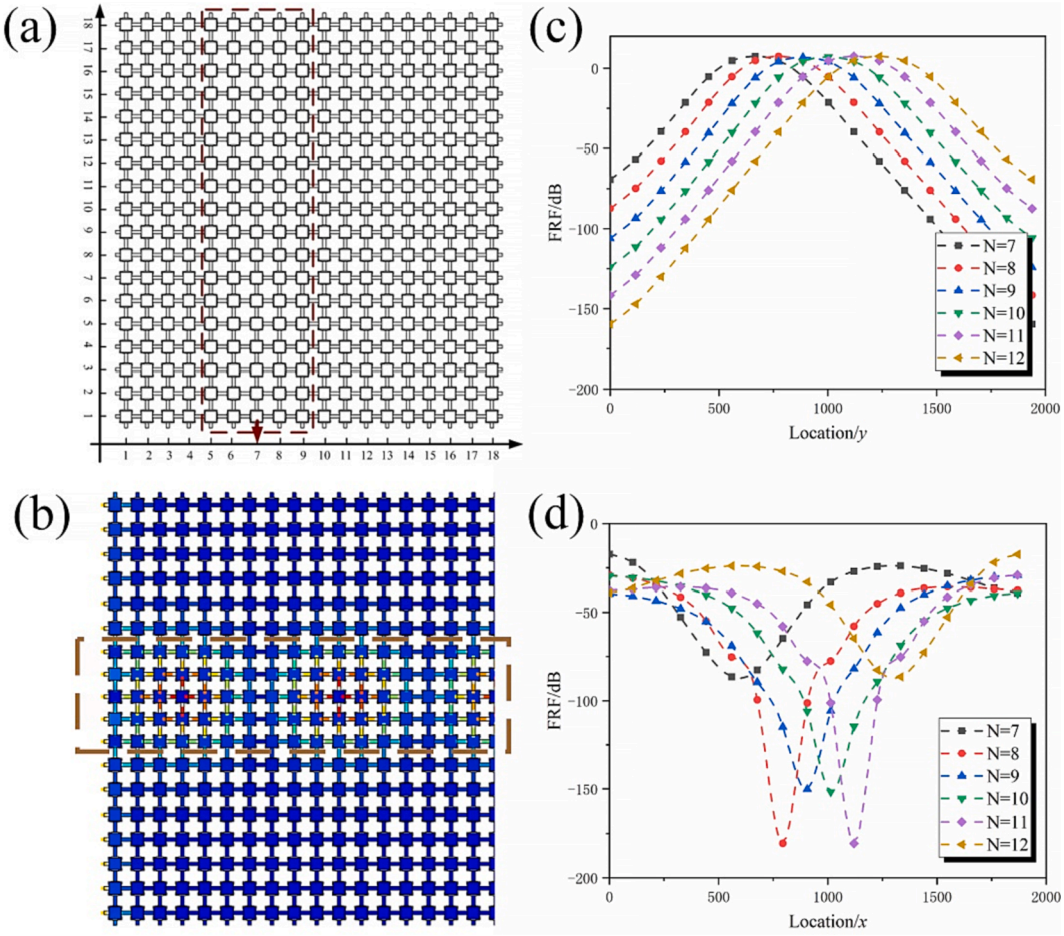

Fig. 9. (a) Waveguide with 18 × 18 Units and (b) Displacement Distribution for N = 10 and FRF Curves (c) along y-direction at 590 Hz and (d) along x-direction at 612 Hz.

propagate only along the waveguide at state 00. In the *x*-direction, the wave at 612 Hz can propagate in state 01, but not in state 11. Applying an external force in the *x*-direction alters the waveguide position. The calculation results in Fig. 9(d) reveal that the wave at 612 Hz can propagate only along the waveguide in state 01. The REMs proposed in this study facilitate the modulation of elastic waves through force application at certain positions in two directions, a property which is beneficial for the design of various functional waveguides.

4. Conclusion

In this study, 2D reconfigurable metamaterials with multiple stable states are designed based on a bending beam structure, which possessed three stable structural forms (states 00, 01, and 11). Each of these three configurations is shown to have a different band structures. Vibration mode analysis reveals that the bandgap of the described REM is defined by local resonance effects. More specifically, the first bandgap is caused by *translational motion*, whereas the second and third bandgaps are caused by *rotation*. The propagation characteristics of elastic waves in different stable states enable these materials to be used in elastic waveguide switches that can interchange between states when different forces are applied, allowing for the modulation of elastic wave propagation behavior at subwavelength. Compared with previous works, the novel REMs described in this study have more design freedom, allowing for finer tuning of elastic wave propagation. The REMs discussed in this study are excellent materials to be used when designing broadband vibration-isolation devices. A waveguide is also designed, allowing for wave propagation to be controlled through the application of external forces in different directions. The methods described in this paper represent a novel approach for designing reconfigurable elastic wave materials, elastic wave logic circuits, and waveguides.

CRediT authorship contribution statement

Meng Chen: Conceptualization, Software, Writing – original draft. **Boya Xiao:** Software, Validation. **Yafei Feng:** Data curation, Formal analysis. **Tao Yang:** Software, Visualization. **Han Zhang:** Formal analysis. **Yu Liu:** Visualization, Investigation. **Wenshuai Xu:** Visualization. **Heng Jiang:** Writing – review & editing. **Yuren Wang:** Supervision.

Declaration of Competing Interest

The authors declare that they have no known competing financial interests or personal relationships that could have appeared to influence the work reported in this paper.

Data availability

Data will be made available on request.

Acknowledgements

This research was funded by the National Natural Science Foundation of China (Grants#11972034 and #11802213), and the Youth Innovation Promotion Association of the Chinese Academy of Science (Grant #2020018).

Appendix A. Supplementary material

Supplementary data to this article can be found online at https://doi.org/10.1016/j.engstruct.2023.115715.

References

[1] Liu Z, Zhang X, Mao Y, Zhu YY, Yang Z, Chan CT, et al. Locally resonant sonic materials. Science 2000;289(5485):1734–6.
[2] Liu XN, Hu GK, Huang GL, Sun CT. An elastic metamaterial with simultaneously negative mass density and bulk modulus. Appl Phys Lett 2011;98(25):251907.
[3] Lai Y, Wu Y, Sheng P, Zhang ZQ. Hybrid elastic solids. Nat Mater 2011;10(8):620–4.
[4] Wu Y, Lai Y, Zhang ZQ. Elastic metamaterials with simultaneously negative effective shear modulus and mass density. Phys Rev Lett 2011;107(10):105506.
[5] Zhu R, Liu XN, Hu GK, Sun CT, Huang GL. Negative refraction of elastic waves at the deep-subwavelength scale in a single-phase metamaterial. Nat Commun 2014;5(1):1–8.
[6] Park J, Lee D, Rho J. Recent advances in non-traditional elastic wave manipulation by macroscopic artificial structures. Appl Sci 2020;10(2):547.
[7] Wu L, Wang Y, Chuang K, Wu F, Wang Q, Lin W, et al. A brief review of dynamic mechanical metamaterials for mechanical energy manipulation. Mater Today 2021;44:168–93.
[8] Wang G, Yu D, Wen J, Liu Y, Wen X. One-dimensional phononic crystals with locally resonant structures. Phys Lett A 2004;327(5–6):512–21.
[9] Hirsekorn M, Delsanto PP, Leung AC, Matic P. Elastic wave propagation in locally resonant sonic material: comparison between local interaction simulation approach and modal analysis. J Appl Phys 2006;99(12):124912.
[10] Liu Z, Chan CT, Sheng P. Analytic model of phononic crystals with local resonances. Phys Rev B 2005;71(1):014103.
[11] D'Alessandro L, Belloni E, Ardito R, Corigliano A, Braghin F. Modeling and experimental verification of an ultra-wide bandgap in 3D phononic crystal. Appl Phys Lett 2016;109(22):221907.
[12] Pennec Y, Djafari-Rouhani B, Larabi H, Vasseur J, Hladky-Hennion AC. Phononic crystals and manipulation of sound. Phys Status Solidi (c) 2009;6(9):2080–5.
[13] Badreddine Assouar M, Senesi M, Oudich M, Ruzzene M, Hou Z. Broadband plate-type acoustic metamaterial for low-frequency sound attenuation. Appl Phys Lett 2012;101(17):173505.
[14] Chen Y, Wang L. Periodic co-continuous acoustic metamaterials with overlapping locally resonant and Bragg band gaps. Appl Phys Lett 2014;105(19):191907.
[15] Phani AS, Woodhouse J, Fleck NA. Wave propagation in two-dimensional periodic lattices. J Acoust Soc AM 2006;119(4):1995–2005.
[16] Ruzzene M, Scarpa F, Soranna F. Wave beaming effects in two-dimensional cellular structures. Smatr Mater Struct 2003;12(3):363–72.
[17] Wang YF, Wang YS, Zhang C. Bandgaps and directional properties of two-dimensional square beam-like zigzag lattices. Aip Adv 2014;4(12):124403.
[18] Yang CL, Zhao SD, Wang YS. Experimental evidence of large complete bandgaps in zig-zag lattice structures. Ultrasonics 2017;74:99–105.
[19] Sigalas M, Economou EN. Band structure of elastic waves in two dimensional systems. Solid State Commun 1993;86(3):141–3.
[20] Kushwaha MS, Halevi P, Dobrzynski L, Djafari-Rouhani B. Acoustic band structure of periodic elastic composites. Phys Rev Lett 1993;71(13):2022–5.
[21] Rupin M, Lemoult F, Lerosey G, Roux P. Experimental demonstration of ordered and disordered multiresonant metamaterials for lamb waves. Phys Rev Lett 2014;112(23):234301.
[22] Yilmaz C, Hulbert GM, Kikuchi N. Phononic band gaps induced by inertial amplification in periodic media. Phys Rev B 2007;76(5):054309.
[23] Hussein MI, Leamy MJ, Ruzzene M. Dynamics of phononic materials and structures: historical origins, recent progress, and future outlook. Appl Mech Rev 2014;66(4):040802.
[24] Xu KF, Zhang YW, Zang J, Niu MQ, Chen LQ. Integration of vibration control and energy harvesting for whole-spacecraft: experiments and theory. Mech Syst Signal Pr 2021;161:107956.
[25] Hu G, Tang L, Liang J, Lan C, Das R. Acoustic-elastic metamaterials and phononic crystals for energy harvesting: a review. Smatr Mater Struct 2021;30(8):085025.
[26] Ma G, Sheng P. Acoustic metamaterials: from local resonances to broad horizons. Sci Adv 2016;2(2):e1501595.
[27] Chen S, Fan Y, Fu Q, Wu H, Jin Y, Zheng J, et al. A review of tunable acoustic metamaterials. App Sci 2018;8(9):1480.
[28] Wang Y, Wang Y, Wu B, Chen W, Wang Y. Tunable and Active Phononic Crystals and Metamaterials. Appl Mech Rev 2020;72(4):040801.
[29] Zhou X, Wang Y, Zhang C. Effects of material parameters on elastic band gaps of two-dimensional solid phononic crystals. J ApplPhys 2009;106:014903.
[30] Ma T, Su X, Wang Y, Wang Y. Effects of material parameters on elastic band gaps of three-dimensional solid phononic crystals. Phys Scr 2013;87:055604.
[31] Zhang X, Liu Z, Liu Y, Wu F. Elastic wave band gaps for three-dimensional phononic crystals with two structural units. Phys Lett A 2003;313:455–60.
[32] Kuang W, Hou Z, Liu Y. The effects of shapes and symmetries of scatterers on the phononic band gap in 2D phononic crystals. Phys Lett A 2004;332:481–90.
[33] Borcea L, Bruno O. On the magneto-elastic properties of elastomer–ferromagnet composites. J Mech Phys Solids 2001;49(12):2877–919.
[34] Chen X, Xu X, Ai S, Chen H, Pei Y, Zhou X. Active acoustic metamaterials with tunable effective mass density by gradient magnetic fields. Appl Phys Lett 2014;105(7):071913.
[35] Chen YY, Huang G. Active elastic metamaterials for subwavelength wave propagation control. Acta Mech Sinica 2015;31(3):349–63.
[36] Sugino C, Leadenham S, Ruzzene M, Erturk A. An investigation of electroelastic bandgap formation in locally resonant piezoelectric metastructures. Smatr Mater Struct 2017;26(5):055029.
[37] Lin Q, Zhou J, Pan H, Xu D, Wen G. Numerical and experimental investigations on tunable low-frequency locally resonant metamaterials. Acta Mech Sinica 2021;34(5):612–23.
[38] Liu H, Zhang Q, Zhang K, Hu G, Duan H. Designing 3D digital metamaterial for elastic waves: from elastic wave polarizer to vibration control. Adv Sci 2019;6(16):1900401.
[39] Lee KH, Yu K, Al Ba'ba'a H, Xin A, Feng Z, Wang Q. Sharkskin-inspired magnetoactive reconfigurable acoustic metamaterials. Research 2020;2020:4825185.
[40] Spadoni A, Daraio C. Generation and control of sound bullets with a nonlinear acoustic lens. Proc Natl Acad Sci USA 2010;107(16):7230–4.
[41] Li F, Anzel P, Yang J, Kevrekidis PG, Daraio C. Granular acoustic switches and logic elements. Nat Commun 2014;5(1):1–6.
[42] Lydon J, Serra-Garcia M, Daraio C. Local to extended transitions of resonant defect modes. Phys Rev Lett 2014;113(18):185503.
[43] Bertoldi K, Boyce MC. Wave propagation and instabilities in monolithic and periodically structured elastomeric materials undergoing large deformations. Phys Rev B 2008;78(18):184107.
[44] Zhang H, Cheng X, Yan D, Zhang Y, Fang D. A nonlinear mechanics model of soft network metamaterials with unusual swelling behavior and tunable phononic band gaps. Compos Sci Technol 2019;183:107822.
[45] Wang P, Casadei F, Shan S, Weaver JC, Bertoldi K. Harnessing buckling to design tunable locally resonant acoustic metamaterials. Phys Rev Lett 2014;113(1):014301.
[46] Bertoldi K, Boyce MC. Mechanically triggered transformations of phononic band gaps in periodic elastomeric structures. Phys Rev B 2008;77(5):052105.
[47] Huang Y, Li J, Chen W, Bao R. Tunable bandgaps in soft phononic plates with spring-mass-like resonators. Int J Mech Sci 2019;151:300–13.
[48] Ren Z, Ji L, Tao R, Chen M, Wan Z, Zhao Z, et al. SMP-based multi-stable mechanical metamaterials: from bandgap tuning to wave logic gates. Extreme Mech Lett 2021;42:101077.
[49] Yu X, Zhou J, Liang H, Jiang Z, Wu L. Mechanical metamaterials associated with stiffness, rigidity and compressibility: a brief review. Prog Mater Sci 2018;94:114–73.
[50] Zhang Y, Li B, Zheng QS, Genin GM, Chen CQ. Programmable and robust static topological solitons in mechanical metamaterials. Nat Commun 2019;10(1):1–8.
[51] Tan X, Zhu S, Wang B, Yao K, Chen S, Xu P, et al. Mechanical response of negative stiffness truncated-conical shell systems: experiment, numerical simulation and empirical model. Compos Part B-Eng 2020;188:107898.
[52] Wu L, Liu L, Wang Y, Zhai Z, Zhuang H, Krishnaraju D, et al. A machine learning-based method to design modular metamaterials. Extreme Mech Lett 2020;36:100657.
[53] Zhai Z, Wang Y, Jiang H. Origami-inspired, on-demand deployable and collapsible mechanical metamaterials with tunable stiffness. Proc Natl Acad Sci USA 2018;115(9):2032–7.
[54] Frazier MJ, Kochmann DM. Band gap transmission in periodic bistable mechanical systems. J Sound Vib 2017;388:315–26.
[55] Kochmann DM, Bertoldi K. Exploiting microstructural instabilities in solids and structures: from metamaterials to structural transitions. Appl Mech Rev 2017;69:050801.
[56] Wu Z, Zheng Y, Wang KW. Metastable modular metastructures for on-demand reconfiguration of band structures and nonreciprocal wave propagation. Phys Rev E 2018;97:022209.
[57] Meaud J, Che K. Tuning elastic wave propagation in multistable architected materials. Int J Solids Struct 2017;122:69–80.
[58] Bilal OR, Foehr A, Daraio C. Bistable metamaterial for switching and cascading elastic vibrations. Proc Natl Acad Sci USA 2017;114(18):4603–6.
[59] Valencia C, Restrepo D, Mankame ND, Zavattieri PD, Gomez J. Computational characterization of the wave propagation behavior of multi-stable periodic cellular materials. Extreme Mech Lett 2019;33:100565.
[60] Goldsberry BM, Haberman MR. Negative stiffness honeycombs as tunable elastic metamaterials. J Appl Phys 2018;123(9):091711.
[61] Hu W, Ren Z, Wan Z, Qi D, Cao X, Li Z, et al. Deformation behavior and band gap switching function of 4D printed multi-stable metamaterials. Mater Design 2021;200:109481.
[62] Ramakrishnan V, Frazier MJ. Multistable metamaterial on elastic foundation enables tunable morphology for elastic wave control. J Appl Phys 2020;127(22):225104.
[63] Meaud J. Multistable two-dimensional spring-mass lattices with tunable band gaps and wave directionality. J Sound Vib 2018;434:44–62.
[64] Schaeffer M, Ruzzene M. Wave propagation in multistable magneto-elastic lattices. Int J Solids Struct 2015;56:78–95.
[65] Liu X, Cai G, Wang K. Synthesizing and reconfiguring metastable modular metamaterials for adaptive wave propagation control. J Sound Vib 2020;468:115114.
[66] Mao J, Wang S, Tan W, Liu M. Modular multistable metamaterials with reprogrammable mechanical properties. Eng Struct 2022;272:114976.
[67] Qiu J, Lang JH, Slocum AH. A curved-beam bistable mechanism. J Microelectromech S 2004;13(2):137–46.

[68] Hua J, Lei H, Zhang Z, Gao C, Fang D. Multistable cylindrical mechanical metastructures: theoretical and experimental studies. J Appl Mech 2019;86(7):071007-1.
[69] Veres IA, Berer T, Matsuda O. Complex band structures of two dimensional phononic crystals: analysis by the finite element method. J Appl Phys 2013;114(8):083519.
[70] Oudich M, Li Y, Assouar BM, Hou Z. A sonic band gap based on the locally resonant phononic plates with stubs. New J Phys 2010;12(8):083049.
[71] Wang Y, Wang Y, Zhang C. Two-dimensional locally resonant elastic metamaterials with chiral comb-like interlayers: bandgap and simultaneously double negative properties. J Acoust Soc Am 2016;139(6):3311–9.
[72] Wang G, Shao L, Liu Y, Wen J. Accurate evaluation of lowest band gaps in ternary locally resonant phononic crystals. Chin Phys 2006;15(8):1843–8.